# Journal of Materials Chemistry A

Accepted Manuscript






ROYAL SOCIETY OF CHEMISTRY

www.rsc.org/materialsA

Journal Name

ARTICLE

# Exceptional size-dependent catalytic activity enhancement in the room-temperature hydrogen generation from formic acid over bimetallic nanoparticles supported by porous carbon

Received 00th January 20xx,
Accepted 00th January 20xx

DOI: 10.1039/x0xx00000x

www.rsc.org/

Jia Cheng, Xiaojun Gu,* Xueli Sheng, Penglong Liu and Haiquan Su*

In this work, we reported a prominent size-dependent activity in the catalytic dehydrogenation of formic acid (HCOOH, FA) over carbon-supported AuPd alloy nanoparticles (NPs) directed by amino acids (lysine, serine and glutamic acid) with different isoelectric points. Through decreasing the average size of AuPd NPs from 12.8 ± 0.5 to 3.8 ± 0.5 nm using different amino acids as structure-directing agents, the drastic activity enhancement in the generation of hydrogen without CO impurity from FA was observed, and the initial turnover frequency (TOF) value was enhanced from 14 to 718 $h^{-1}$ at 298 K, which was among the highest values for the reported heterogeneous catalysts for FA dehydrogenation under the same conditions. Through optimizing the molar ratio of Au/Pd and the metal loading in the catalysts, the initial TOF value for FA dehydrogenation was enhanced to 1153 $h^{-1}$ at 298 K. In addition, the catalyst with the smallest size of AuPd NPs gave an initial TOF value of 2972 $h^{-1}$ at 323 K with 100 % $H_2$ selectivity, comparable to the values acquired from the most active homogeneous catalysts. The investigation of UV-vis spectroscopy showed that the reaction between mixed metal ions ($Pd^{2+}$ and $AuCl_4^-$) and three amino acids before the reduction of $NaBH_4$ leaded to the formation of three different coordination complex intermediates, which induced the formation of different-sized AuPd alloy NPs featuring remarkably different catalytic performance on FA dehydrogenation.

## 1. Introduction

Hydrogen has attracted considerable attention as an ideal alternative to petrochemical energy.[1] Currently, searching for effective hydrogen storage materials and methods for hydrogen generation in safe and efficient ways remains one of the most difficult challenges toward a fuel-cell-based hydrogen economy.[2] Formic acid (HCOOH, FA) is a promising hydrogen carrier since it has high energy density and can be obtained by biomass processing and artificial photocatalytic $CO_2$ reduction.[3] For hydrogen-based energy application, it is desirable to develop high-performance catalysts for FA dehydrogenation ($HCOOH \rightarrow CO_2 + H_2$, $\Delta G$ = −48.4 kJ $mol^{-1}$) at mild conditions, especially at room temperature, and in the meantime, the undesirable dehydration reaction should be avoided since dehydration-generated CO ($HCOOH \rightarrow CO + H_2O$, $\Delta G$ = −28.5 kJ $mol^{-1}$) is a fatal poison to the catalysts of fuel cells.[4] Compared to monometallic catalysts, bimetallic catalysts such as supported alloy nanoparticles (NPs) have preferable catalytic performance by the synergistic interaction between two different metals in terms of the ensemble effect and the ligand effect.[5,6] Although some progress has been achieved in this aspect, there is still no remarkable enhancement on the catalytic activities of bimetallic NPs even at elevated temperature up to 363 K.[2d,7]

For heterogenerous catalysis, the particle size of active components usually significantly correlates with their surface area and the percentages of different crystal facets, which has potential impact on the catalytic activity and selectivity of target product.[8,9] However, to date, the particle-size effect of bimetallic alloy NPs on the remarkable enhancement in the catalytic activity of FA dehydrogenation has been rarely studied systematically, most probably due to the big challenge in synthesizing active bimetallic alloy NPs with well-controlled sizes. Traditionally, alloy NPs have been prepared mainly in the presence of surfactants with long hydrocarbon chains such as hexadecyltrimethylammonium bromide (CTAB).[10] However, the protective surfactants easily occupy much of the active sites of the NPs and then are unfavorable for catalytic applications.[11] Therefore, it is urgently desirable to construct catalysts based on surfactant-free alloy NPs with controlled particle size for remarkably enhancing the activity of FA dehydrogenation at room temperature.

Herein, we reported a size-dependent activity in the hydrogen generation from FA over AuPd nanocatalysts. Surprisingly, through decreasing the size of carbon-supported AuPd alloy NPs using different amino acids (lysine, serine and glutamic acid) as structure-directing agents, the activity and $H_2$

*Inner Mongolia Key Laboratory of Coal Chemistry, School of Chemistry and Chemical Engineering, Inner Mongolia University, Hohhot 010021, China. E-mail: xiaojun.gu@yahoo.com, haiquansu@yahoo.com; Fax: +86-471-499-2981; Tel: +86-471-499-2981*

† Electronic Supplementary Information (ESI) available: Synthesis of catalysts, ICP, TEM, XRD, IR, BET, XPS, and TOF values; the experimental results for hydrogen generation from FA. See DOI: 10.1039/x0xx00000x

selectivity of FA decomposition were drastically enhanced at 298 K. Moreover, the origination of remarkably different activities of AuPd NPs directed by different amino acids was discovered using UV-vis spectroscopy.

## 2. Experimental section

### 2.1 Chemicals

All chemicals were commercial and used without further purification. Formic acid (HCOOH, Sigma-Aldrich, 99%), sodium formate (HCOONa, Sigma-Aldrich, >99%), palladium chloride ($PdCl_2$, Sinopharm Chemical Reagent Co., Ltd, >99%), tetrachloroauric acid ($HAuCl_4{\cdot}4H_2O$, Sinopharm Chemical Reagent Co., Ltd, >99%), sodium borohydride ($NaBH_4$, J&K Chemical, 99%), lysine (J&K Chemical, 99%), serine (Sigma-Aldrich, 99%), glutamic acid (Sigma-Aldrich, 99%), Vulcan XC-72 carbon (Cabot Chemical Co., Ltd), sodium hydroxide (NaOH, Sinopharm Chemical Reagent Co., Ltd, >99%), hexadecyltrimethylammonium bromide (Sinopharm Chemical Reagent Co., Ltd, 99% ), and methanol ($CH_3OH$, Tianjin Fengchuan Chemical Reagent Technologies Co., Ltd, >99%) were used. Deionized $H_2O$ was used in all experiments.

### 2.2 Synthesis and catalytic study

All the catalysts were synthesized using an impregnation-reduction process. For the synthesis of $Au_{0.75}Pd_{0.25}$/C-L-7.5 (L = lysine, C = Vulcan XC-72 carbon) with 7.5 of the molar ratio of lysine/metal, $HAuCl_4{\cdot}4H_2O$ (0.1064 g, 0.258 mmol) and $PdCl_2$ (0.0152 g, 0.086 mmol) were dispersed in 40 mL of methanol with sonication for 3 h. And then activated carbon (0.24 g) was added into the above mixture. Two hours later, lysine (0.377 g, 2.58 mmol) in 150 mL of deionized $H_2O$ was added into the suspension. After 2 hours, 30 mL of methanol solution containing 0.26 g of $NaBH_4$ was added into the above mixture. Keep stirring for 4 hours, and the product was obtained by centrifugation (5000 rpm/min), washed with methanol and deionized $H_2O$ for several times, and finally dried in vacuum oven at 80 $^{o}$C to yield the catalyst $Au_{0.75}Pd_{0.25}$/C-L-7.5. For the synthesis of $Au_{0.75}Pd_{0.25}$/C-S-7.5 (S = serine) and $Au_{0.75}Pd_{0.25}$/C-G-7.5 (G = glutamic acid), the process was same as that for $Au_{0.75}Pd_{0.25}$/C-L-7.5 except for the utilization of serine and glutamic acid as structure-directing agents, resepctively.

Through tuning the molar ratios of Au/Pd, metal loadings, molar ratios of amino acid/metal and structur-directing agents such as CTAB and NaOH, other nineteen catalysts, $Au_{0.75}Pd_{0.25}$/C-L-7.5 with 10 wt% of metal loading, $Au_{0.5}Pd_{0.5}$/C-L-7.5, $Au_{0.5}Pd_{0.5}$/C-L-7.5 with 10 wt% of metal loading, $Au_{0.67}Pd_{0.33}$/C-L-7.5, $Au_{0.67}Pd_{0.33}$/C-L-7.5 with 10 wt% of metal loading, $Au_{0.33}Pd_{0.67}$/C-L-7.5, $Au_{0.33}Pd_{0.67}$/C-L-7.5 with 10 wt% of metal loading, $Au_{0.25}Pd_{0.75}$/C-L-7.5, $Au_{0.25}Pd_{0.75}$/C-L-7.5 with 10 wt% of metal loading, $Au_{0.75}Pd_{0.25}$/C-L-3.5, $Au_{0.75}Pd_{0.25}$/C-L-10, CTAB-directed $Au_{0.75}Pd_{0.25}$/C, NaOH-directed $Au_{0.75}Pd_{0.25}$/C, $Au_{0.75}Pd_{0.25}$/C, Au/C-L-7.5, Pd/C-L-7.5, Pd/C-S-7.5, Pd/C-G-7.5 and Pd/C were synthesized using the similar process for $Au_{0.75}Pd_{0.25}$/C-L-7.5 (see Supporting Information).

For the catalytic study, the as-prepared catalyst was kept in a two-necked round-bottom flask. One neck was connected to a gas burette, and the other was connected to a pressure-equalization funnel to introduce aqueous solution containing FA. The catalytic reaction began once the solution containing FA was injected into the flask. The evolution of gas was monitored using the gas burette. The reaction was carried out at different temperatures under ambient atmosphere.

### 2.3 Characterization

Powder X-ray diffraction (XRD) was performed on a Panalytical X-Pert X-ray diffract meter with a Cu-Kα source (40 kV, 20 mA). The surface area measurements were performed by $N_2$ adsorption/desorption at liquid $N_2$ temperature (77 K) after dehydration under vacuum at 150 °C for 12 h using automatic volumetric adsorption equipment (Autosorb-iQ2-MP). The X-ray photoelectron spectra (XPS) were acquired with an ESCALAB250 (Thermo VG Corp.) equipped with an Al-Kα X-ray excitation source (1486.6 eV) that operated at 15 kV and 20 mA. The morphologies and sizes of all of the samples were observed using a transmission electron microscopy (TEM, JEM-2010). TEM samples were prepared by depositing one or two droplets of the catalyst suspensions onto amorphous carbon-coated copper grids. Inductively coupled plasma-atomic emission spectroscopy (ICP-AES) measurement was performed on a Thermo Jarrell Ash (TJA) Atomscan Advantage instrument. Detailed analyses for $CO_2$, $H_2$ and CO were performed on Shimadzu GC-2014 with thermal conductivity detector (TCD) and hydrogen flame ionization detector (FID)-Methanator (detection limit: 10 ppm). The IR spectra were recorded on an infrared spectrometer (Thermo Fisher Scientific, NEXUS-670) in the wavenumber range from 400–4000 $cm^{-1}$. The UV-vis spectra were conducted on a Shimadzu UV-3600.

## 3. Results and discussion

In order to explore the size effect of AuPd NPs on FA dehydrogenation, three amino acids including lysine, serine and glutamic acid were selected to direct the synthesis of carbon-supported catalysts with different sizes of AuPd NPs. These water soluble amino acids with low molecular weight could be easily removed from the as-synthesized catalysts, and thus the surface of AuPd NPs could be free and clean, which was crucial for catalysis.

The method for synthesizing AuPd alloy NPs was shown in Fig 1. When the basic lysine was selected, the $NH_2$ and deprotonated $COO^-$ groups interacted with $AuCl_4^-$ and $Pd^{2+}$ ions through coordination bonds and electrostatic interactions.[12] These strong interactions suppressed the motion of reduced Au and Pd atoms in a nanospace, leading to the formation of AuPd alloy NPs with small size. When acidic glutamic acid was used, the weak immobilization for $Pd^{2+}$ and $AuCl_4^-$ ions resulted in the formation of AuPd alloy NPs with big size due to the undeprotonation of COOH group in the non-α-site of carbon in glutamic acid. When natural serine was used, the size of resulting AuPd alloy NPs fell in the size range of AuPd NPs induced by lysine and glutamic acid due to the absence of $NH_2$ or undeprotonated COOH group in the non-α-site of carbon in serine.



 

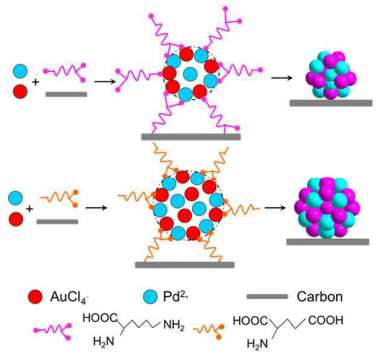


Fig. 1 Schematic illustration for preparation of supported AuPd alloy NPs with different sizes by the assistance of different amino acids.

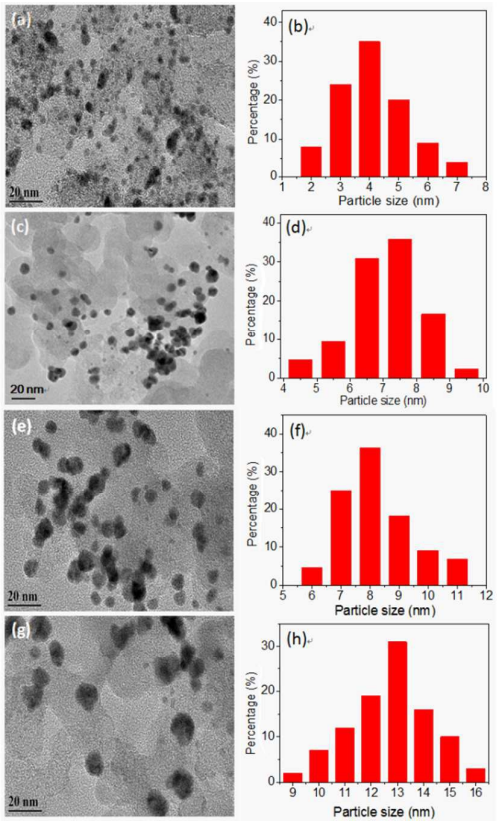


Fig. 2 Representative TEM images of the as-synthesized catalysts and the corresponding size distributions of AuPd NPs: (a, b) $Au_{0.75}Pd_{0.25}$/C-L-7.5; (c, d) $Au_{0.75}Pd_{0.25}$/C; (e, f) $Au_{0.75}Pd_{0.25}$/C-S-7.5; (g, h) $Au_{0.75}Pd_{0.25}$/C-G-7.5.

TEM was used to characterize the size evolution of AuPd NPs directed by different amino acids. As shown in Fig. 2, AuPd NPs in $Au_{0.75}Pd_{0.25}$/C-L-7.5 were dispersed on carbon with an average particle size of 3.8 ± 0.5 nm despite very few aggregated NPs being observed. The high-resolution TEM (HRTEM) image showed the crystalline nature of AuPd NPs with (111) lattice fringe distance of 0.230 nm (Fig. S1), which was between the lattice spacing of face-centered cubic (fcc) Au (0.235 nm) and Pd (0.225 nm). In sharp contrast, AuPd NPs in $Au_{0.75}Pd_{0.25}$/C, $Au_{0.75}Pd_{0.25}$/C-S-7.5 and $Au_{0.75}Pd_{0.25}$/C-G-7.5 showed big average sizes of 7.2 ± 0.5, 7.8 ± 0.5 and 12.8 ± 0.5 nm, respectively. From these TEM results, it could be concluded that the different particle sizes were caused by different abilities of amino acids for immobilizing AuPd NPs, leading to different catalytic performance on FA dehydrogenation as below. The XRD pattern of every nanocatalyst only exhibited a peak between the characteristic peaks for Au (111) and Pd (111), indicating the formation of AuPd alloy (Fig. S2).[2d,7] The investigation of XPS showed that the binding energies of Pd 3d in $Au_{0.75}Pd_{0.25}$/C-L-7.5 were shifted to the lower values compared to those in Pd/C-L-7.5, while the binding energies of Au 4f in $Au_{0.75}Pd_{0.25}$/C-L-7.5 were shifted to the higher values compared to those in Au/C-L-7.5 (Fig. 3). These shifts demonstrated that some electrons were transferred from Au to Pd atom in the alloy structure of AuPd NPs.[13] Such electron transfer in $Au_{0.75}Pd_{0.25}$/C-L-7.5 had the potential to endow itself with the high activity in the hydrogen generation from FA at 298 K. The Brunauer-Emmertt-Teller (BET) surface areas of support carbon and catalyst $Au_{0.75}Pd_{0.25}$/C-L-7.5 were 228 and 128 $cm^3 \cdot g^{-1}$, respectively (Fig. S5). The appreciable decrease in the amount of $N_2$ adsorption of catalyst indicated that the channels of porous carbon were occupied by AuPd NPs and/or blocked by the AuPd NPs located at their surface. The IR spectra showed that there was no $NH_2$ group in the three as-synthesized catalysts (Fig. S6), indicating that the amino acids were completely removed from the catalysts.

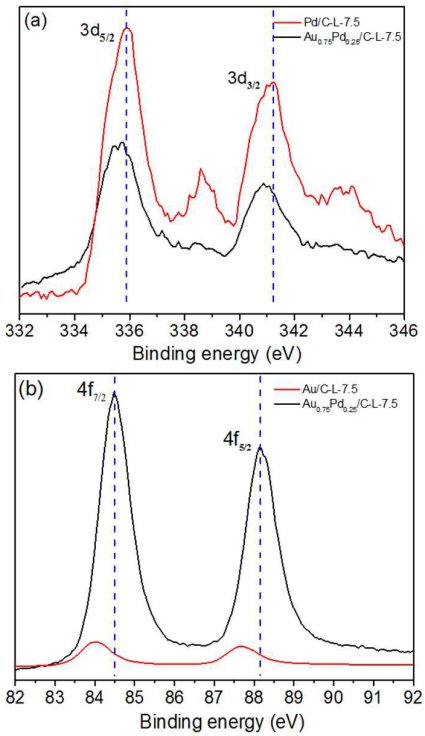


Fig. 3 XPS spectra in (a) Pd 3d regions of Pd/C-L-7.5 and $Au_{0.75}Pd_{0.25}$/C-L-7.5 and (b) Au 4f regions of Au/C-7.5 and $Au_{0.75}Pd_{0.25}$/C-L-7.5.

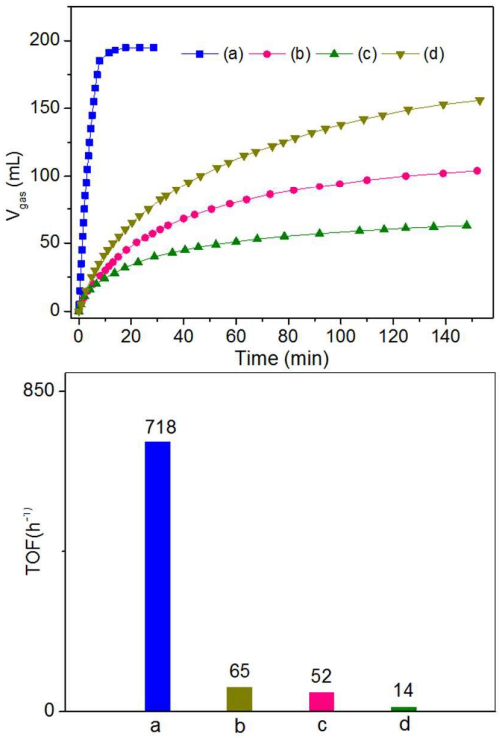


Fig. 4 (Top) Plots of time versus volume of generated gas ($CO_2$ and $H_2$) from FA-SF aqueous solution (FA/SF = 1:1, FA = 1.0 M, 3.5 mL) over 50 mg of (a) $Au_{0.75}Pd_{0.25}$/C-L-7.5, (b) $Au_{0.75}Pd_{0.25}$/C, (c) $Au_{0.75}Pd_{0.25}$/C-S-7.5 and (d) $Au_{0.75}Pd_{0.25}$/C-G-7.5 at 298 K and (bottom) TOF values for FA dehydrogenation over the above four catalysts at 298 K.

To examine the dependence of the FA dehydrogenation activity on the controlled sizes of AuPd NPs, four catalysts $Au_{0.75}Pd_{0.25}$/C-L-7.5, $Au_{0.75}Pd_{0.25}$/C-S-7.5, $Au_{0.75}Pd_{0.25}$/C-G-7.5 and $Au_{0.75}Pd_{0.25}$/C were used to check the hydrogen production performance. To our surprise, lysine-directed $Au_{0.75}Pd_{0.25}$/C-L-7.5 exhibited a high activity and 100% of $H_2$ selectivity in a FA-sodium formate (SF) solution at 298 K (Fig. 4). The GC analysis confirmed that no CO existed in the mixture of $H_2$ and $CO_2$ generated in FA decomposition (Fig. 5a), which was crucial for fuel cell applications.[2,3] Moreover, the GC analysis confirmed equal molar amount of $CO_2$ and $H_2$ in the generated gas mixture (Fig. 5b). No gas was detected from the hydrolysis of SF at 298 K (Fig. S7), which again verified that the $Au_{0.75}Pd_{0.25}$/C-L-7.5 promoted complete decomposition of FA into $H_2$ and $CO_2$. Particular noteworthy was that $Au_{0.75}Pd_{0.25}$/C-L-7.5 gave a high turnover frequency (TOF) value of 718 $h^{-1}$ in 30 % of FA conversion, which was among the highest values reported so far under the similar conditions, i.e., Pd/MSC-30 (750 $h^{-1}$ at 298 K),[6a] Au/$ZrO_2$ (252 $h^{-1}$ at 298 K),[4f] Pd/g-$C_3N_4$ (71 $h^{-1}$ at 288 K),[5e] Pd/C-$NaBH_4$ (304 $h^{-1}$ at 303 K)[6b] and Pd-B/C (1184 $h^{-1}$ at 303 K)[6b] (Table S2). In sharp contrast, $Au_{0.75}Pd_{0.25}$/C, $Au_{0.75}Pd_{0.25}$/C-S-7.5 and $Au_{0.75}Pd_{0.25}$/C-G-7.5 only had 80, 53 and 32 % of $H_2$ selectivity, respectively, and gave initial TOF values of 65, 52 and 14 $h^{-1}$, respectively. The above remarkable differences in activities and $H_2$ selectivity could be related to the different sizes of AuPd NPs in these catalysts directed by different amino acids. In addition, compared to Pd/C-L-7.5 with low activity and Au/C-L-7.5 with no activity, $Au_{0.75}Pd_{0.25}$/C-L-7.5 exhibited the high activity (Fig. S8), indicating the synergetic effect between Pd and Au in the activity enhancement of AuPd alloy catalyst.

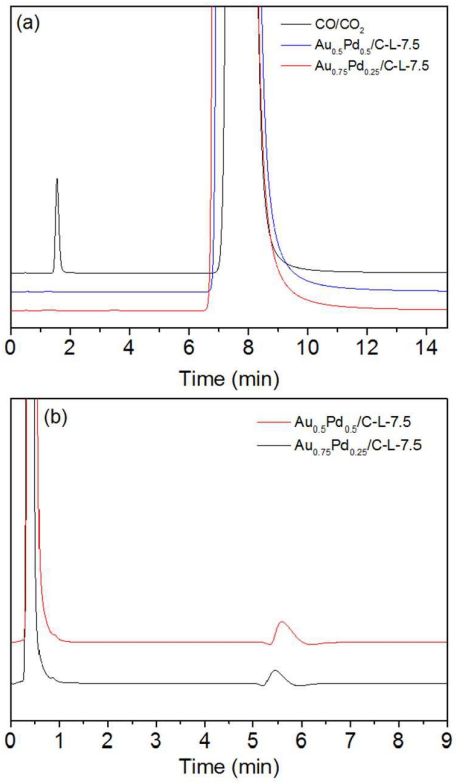


Fig. 5 GC spectra obtained using (a) FID-Methanator for the mixture of CO and $CO_2$ with 100 ppm of CO and the evolved gas and (b) TCD for the evolved gas from FA-SF aqueous solution (FA/SF = 1:1, FA = 1.0 M, 3.5 mL) over 50 mg of $Au_{0.75}Pd_{0.25}$/C-L-7.5 and $Au_{0.5}Pd_{0.5}$/C-L-7.5 at 298 K.

Generally, the molar ratio of ligand/metal has influenced the structures of resulting coordination complexes.[14] If these different coordination complexes are used as precursors of metal NPs, the metal NPs with different morphologies such as size could be obtained. From this viewpoint, various molar ratios of lysine/metal such as 3.5 and 10 were selected to synthesize two catalysts labeled as $Au_{0.75}Pd_{0.25}$/C-L-3.5 and $Au_{0.75}Pd_{0.25}$/C-L-10. The TEM results showed that the average sizes of AuPd NPs in $Au_{0.75}Pd_{0.25}$/C-L-3.5 and $Au_{0.75}Pd_{0.25}$/C-L-10 were 4.4 $\pm$ 0.5 and 5.8 $\pm$ 0.5 nm, respectively (Fig. S9 and S10). As expected that both catalysts had 100% of $H_2$ selectivities and $Au_{0.75}Pd_{0.25}$/C-L-3.5 had higher activity than $Au_{0.75}Pd_{0.25}$/C-L-10 (Fig S11). However, both catalysts had lower activities than $Au_{0.75}Pd_{0.25}$/C-L-7.5, where AuPd NPs featured an average size of 3.8 $\pm$ 0.5 nm.

The catalytic performance was optimized by tuning the molar ratio of Au/Pd and metal loadings in the catalysts. Through the comparasion of the catalytic activities of ten

catalysts, namely, $Au_{0.75}Pd_{0.25}$/C-L-7.5, $Au_{0.67}Pd_{0.33}$/C-L-7.5, $Au_{0.5}Pd_{0.5}$/C-L-7.5, $Au_{0.33}Pd_{0.67}$/C-L-7.5, $Au_{0.25}Pd_{0.75}$/C-L-7.5, $Au_{0.75}Pd_{0.25}$/C-L-7.5 with 10 wt% of metal loading, $Au_{0.67}Pd_{0.33}$/C-L-7.5 with 10 wt% of metal loading, $Au_{0.5}Pd_{0.5}$/C-L-7.5 with 10 wt% of metal loading, $Au_{0.33}Pd_{0.67}$/C-L-7.5 with 10 wt% of metal loading and $Au_{0.25}Pd_{0.75}$/C-L-7.5 with 10 wt% of metal loading, it was found that $Au_{0.67}Pd_{0.33}$/C-L-7.5 and $Au_{0.67}Pd_{0.33}$/C-L-7.5 with 10 wt % of metal loading had the highest activities among the AuPd catalysts with the similar metal loadings (Fig. S12 and S13). Especially, $Au_{0.67}Pd_{0.33}$/C-L-7.5 with 10 wt % of metal loading gave a TOF value of 1153 $h^{-1}$ in 30 % of FA conversion at 298 K (Table S2), which was comparable to the values acquired from the most active homogeneous catalysts.[2f] Besides the size of active metal NPs, other factors such as the chemical state of active metal centers can also influence the catalytic performance such as activity of a catalyst. Then the XPS spectra in the Pd 3d regions of amino-acid-directed AuPd catalysts $Au_{0.5}Pd_{0.5}$/C-L-7.5, $Au_{0.5}Pd_{0.5}$/C-L-7.5 with 10 wt% of metal loading, $Au_{0.75}Pd_{0.25}$/C-L-7.5, $Au_{0.75}Pd_{0.25}$/C-S-7.5, $Au_{0.75}Pd_{0.25}$/C-G-7.5, Pd/C-L-7.5, Pd/C-S-7.5 and Pd/C-G-7.5 and amino-acid-free AuPd catalysts $Au_{0.75}Pd_{0.25}$/C and Pd/C were studied in detail. The results showed that there were some differences in the chemical state of Pd active sites in these catalysts (Fig. S14, S15 and S16), which could also account for the different activities of the different catalysts and the resulting enhanced activity of lysine-directed AuPd catalysts as mentioned above. In addition, the reaction rate had a near linear dependency on the FA concentration with a slope of 0.9046 (Fig. 6), indicating that the reaction rate strongly depended on the concentration of FA.

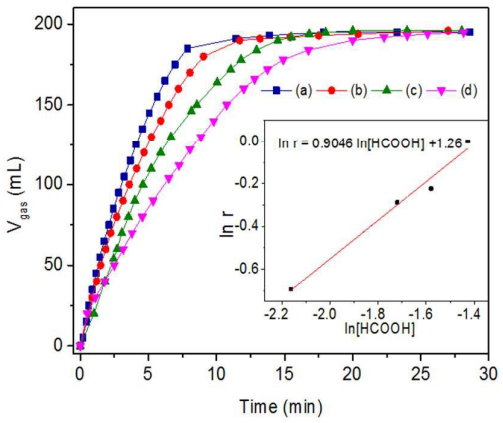


Fig. 6 Plots of time versus volume of generated gas ($CO_2$ and $H_2$) from different FA-SF aqueous solution featuring (a) FA/SF = 1:1, FA = 1.0 M, 3.5 mL, (b) FA/SF = 1:1, FA = 0.8 M, 4.38 mL, (c) FA/SF = 1:1, FA = 0.75 M, 4.67 mL and (d) FA/SF = 1:1, FA = 0.5 M, 7.0 mL over 50 mg of $Au_{0.75}Pd_{0.25}$/C-L-7.5 at 298 K. Insert: the plot of gas generation rate vs FA concentration.

In order to testify that the only basic environment resulted from lysine was not the key factor leading to the high activity of AuPd NPs, the pH value (9.0) equal to that in the synthesis of $Au_{0.75}Pd_{0.25}$/C-L-7.5 was selected to synthesize AuPd catalyst using NaOH as structure-directing agent. The TEM result showed that the average size of AuPd NPs in NaOH-directed catalyst was 11.8 ± 0.5 nm (Fig. 7a and 7b), which was much bigger than that of $Au_{0.75}Pd_{0.25}$/C-L-7.5. This big size of AuPd NPs leaded to the poor activity and only 21 % of $H_2$ selectivity at 298 K (Fig. 8). This indicated that lysine indeed played a key role in the formation of high-performance bimetallic nanocatalyst. In addition, the FA dehydrogenation performance of CTAB-directed AuPd NPs supported on carbon showed that the as-synthesized catalyst almost had no activity despite its small size of AuPd NPs (4.8 ± 0.5 nm) (Fig. 7c, 7d and 8) The observations further confirmed that the absence of protective surfactants with long hydrocarbon chains significantly benefited the access of reaction molecule FA to the surface of AuPd NPs and therefore benefited the enhancement of catalytic performance.

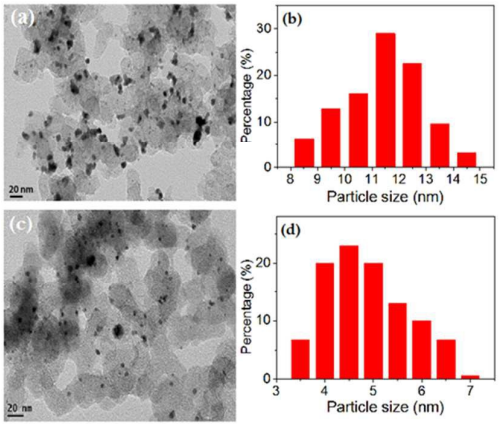


Fig. 7 Representative TEM images of the as-synthesized catalysts and the corresponding size distributions of AuPd NPs: (a, b) NaOH-directed $Au_{0.75}Pd_{0.25}$/C; (c, d) CTAB-directed $Au_{0.75}Pd_{0.25}$/C.

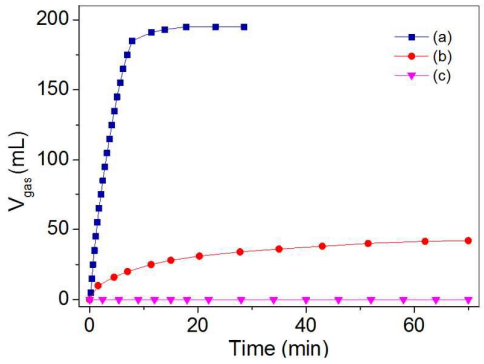


Fig. 8 Plots of time versus volume of generated gas ($CO_2$ and $H_2$) from FA-SF aqueous solution (FA/SF = 1:1, FA = 1.0 M, 3.5 mL) over 50 mg of (a) lysine, (b) NaOH and (c) CTAB-directed $Au_{0.75}Pd_{0.25}$/C at 298 K.

The temperature played an important role in FA dehydrogenation. It could be clearly seen that the hydrogen evolution rate using $Au_{0.75}Pd_{0.25}$/C-L-7.5 as catalyst greatly

depended on the reaction temperature (Fig. 9). The catalyst gave a TOF value of 2972 $h^{-1}$ in 30 % of FA conversion at 323 K, which was comparable to the values acquired from the most active homogeneous catalysts.[2f] According to the Arrhenius plot of ln k versus 1/T, the obtained apparent activation energy ($E_a$) of this process was 42.23 kJ $mol^{-1}$, comparable to most of the reported for heterogeneous FA dehydrogenation.[6] For the stability test, the catalyst $Au_{0.75}Pd_{0.25}$/C-L-7.5 was recycled by additional FA (3.5 mmol) into the reactor after the completion of first run. It was found that the activity and $H_2$ selectivity remained no significant change (Fig. S20), which could be due to the no significant increase in the size of AuPd NPs during the catalytic process (Fig. S21).

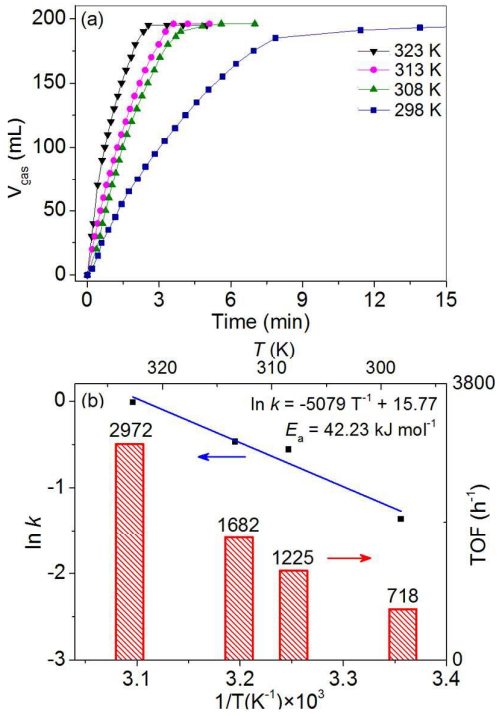


Fig. 9 (a) Plots of time versus volume of generated gas ($CO_2$ and $H_2$) from FA-SF aqueous solution over 50 mg of $Au_{0.75}Pd_{0.25}$/C-L-7.5 at different temperatures and (b) Arrhenius plot and TOF values of FA dehydrogenation over $Au_{0.75}Pd_{0.25}$/C-L-7.5 (FA/SF = 1:1, FA = 1.0 M, 3.5 mL).

Since CO is a fatal poison to the catalysts of fuel cells using $H_2$ as fuel, the influence of CO poisoning on $Au_{0.75}Pd_{0.25}$/C-L-7.5 in the catalytic FA decomposition was also studied. The results showed that the catalyst exposed to CO still had high activity during the FA decomposition (Fig. S22). This high tolerance with respect of CO poisoning was due to the fact that the Au atom, which has weak adsorption strength of CO, effectively inhibited the adsorption of CO on the surface of the active species Pd in the bimetallic catalyst.[2d]

In order to make clear the role of different amino acids in the catalyst formation, we tried to gather insight into the changes of the coordination complex intermediates during the reaction between mixed metal ions ($Pd^{2+}$ and $AuCl_4^-$) and different amino acids using UV-vis spectroscopy, where the molar ratio of amino acid/metal ions was kept at 7.5. To eliminate the disturbance of black carbon, only an aqueous solution of the coordination complex precursors was used. From the UV-vis spectra monitoring the reaction process (Fig. 10), it could be found that three new characteristic peaks at different wavelengths (207, 222, and 202 nm) appeared, which can be attributed to the formation of different coordination complexes in the present of lysine, serine and glutamic acid, respectively. So the three different coordination complex intermediates acted as precursors in the subsequent $NaBH_4$ reduction and induced the formation of AuPd NPs with different sizes, which resulted in the different catalytic performance on FA dehydrogenation at 298 K.

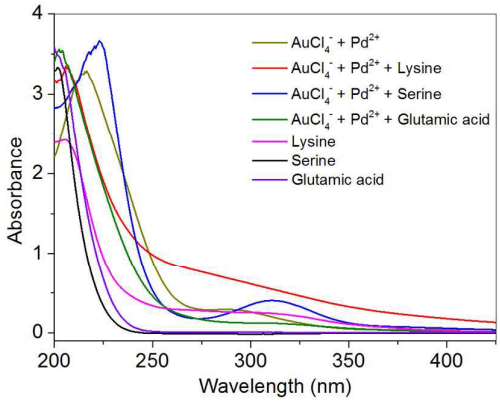


Fig. 10 UV-vis spectra of aqueous solutions containing various species.

## Conclusions

In summary, amino acids with different isoelectric points as structure-directing agents were used to successfully synthesize carbon-supported AuPd alloy NPs with different sizes, which featured the distinct size-dependent catalysis in the production of hydrogen without CO contamination from FA at 298 K. The catalyst with the small particle size of AuPd NPs had the remarkably higher catalytic activity and $H_2$ selectivity than the catalysts with big size of AuPd NPs, which suggested a general strategy for further improvement of catalytic performance of FA dehydrogenation. In addition, three different coordination complex intermediates generated from the reaction between mixed metal ions and three amino acids played an important role in synthesizing AuPd alloy NPs with different sizes. Through exploring the structure-activity relationships for catalysts by a fine tuning of bimetallic NPs in the nanometer size range, it is possible to design high-performance cost-effective nanocatalysis systems that are important for sustainable energy production and chemical synthesis applications.

## Acknowledgements

The authors gratefully acknowledge the financial support from the Program for New Century Excellent Talents in University of

the Ministry of Education of China (grant no. NCET-13-0846), the National Natural Science Foundation of China (grant no. 21101089), the Inner Mongolia Natural Science Foundation (grant no. 2011JQ01) and the Program for Young Talents of Science and Technology in Universities of Inner Mongolia Autonomous Region (grant no. NJYT-13-A01).

## References

1 (*a*) P. P. Edwards, V. L. Kuznetsov, W. I. David and N. P. Brandon, *Energy Policy*, 2008, **36**, 4356–4362; (*b*) J. Graetz, *Chem. Soc. Rev.*, 2009, **38**, 73–82; (*c*) C. W. Hamilton, R. T. Baker, A. Staubiz and I. Manners, *Chem. Soc. Rev.*, 2009, **38**, 279–293; (d) H. M. Chen, C. K. Chen, R. S. Liu, L. Zhang, J. Zhang and D. P. Wilkinson, *Chem. Soc. Rev.*, 2012, **41**, 5654–5671.

2 (*a*) L. Schlapbach and A. Züttel, *Nature*, 2001, **414**, 353−358; (*b*) Z. Xiong, C. K. Yong, G. Wu, P. Chen, W. Shaw, A. Karkamkar, T. Autrey, M. O. Jones, S. R. Johnson, P. P. Edwards and W. I. F. David, *Nat. Mater.*, 2008, **7**, 138−141; (*c*) A. Staubitz, A. P. M. Robertson and I. Manners, *Chem. Rev.*, 2010, **110**, 4079−4124; (*d*) X. Gu, Z.-H. Lu, H.-L. Jiang, T. Akita and Q. Xu, *J. Am. Chem. Soc.*, 2011, **133**, 11822−11825; (*e*) Y. Mahendra and Q. Xu, *Energy Environ. Sci.*, 2012, **5**, 9698−9725; (*f*) Q.-L. Zhu and Q.Xu, *Energy Environ. Sci.*, 2015, **8**, 478−512; (g) K. Kang, X. Gu, L. Guo, P. Liu, X. Sheng, Y. Wu, J. Cheng and H. Su, *Int. J. Hydrogen Energy*, 2015, **40**, 12315−12324; (*h*) L. Guo, X. Gu, K. Kang, Y. Wu, J. Cheng, P. Liu, T. Wang and H. Su, *J. Mater. Chem. A*, 2015, 3, 22807−22815.

3 (*a*) F. Jin, J. Yun, G. Li, A. Kishita, K. Tohji and H. Enomoto, *Green Chem.*, 2008, **10**, 612−615; (*b*) K. Tedsree, T. Li, S. Jones, C. W. A. Chan, K. M. K. Yu, P. A. J. Bagot, E. A. Marquis, G. D. W. Smith and S. C. E. Tsang, *Nat. Nanotechnol.*, 2011, **6**, 302−307; (*c*) S. Zhang, Ö. Metin, D. Su and S. Sun, *Angew. Chem., Int. Ed.*, 2013, **52**, 3681−3684; (*d*) W. Wang, M. Niu, Y. Hou, W. Wu, Z. Liu, Q. Liu, S. Ren and K. N. Marsh, *Green Chem.,* 2014, **16**, 2614−2618; (*e*) S. Lee, H. Ju, R. Machunda, S. Uhm, J. K. Lee, H. J. Lee and J. Lee, *J. Mater. Chem. A*, 2015, **3**, 3029−3034.

4 (*a*) A. Boddien, B. Loges, H. Junge and M. Beller, *ChemSusChem*, 2008, **1**, 751−758. (*b*) C. Fellay, P. J. Dyson and G. Laurenczy, *Angew. Chem., Int. Ed.*, 2008, **47**, 3966−3968; (*c*) M. Ojeda and E. Iglesia, *Angew. Chem., Int. Ed.*, 2009, 48, 4800−4803; (*d*) A. Boddien, B. Loges, F. Gärtner, C. Torborg, K. Fumino, H. Junge, R. Ludwig and M. Beller, *J. Am. Chem. Soc.*, 2010, **132**, 8924−8934; (*e*) A. Boddien, D. Mellmann, F. Gärtner, R. Jackstell, H. Junge, P. J. Dyson, G. Laurenczy, R. Ludwig and M. Beller, *Science*, 2011, **333**, 1733−1736; (*f*) Q.-Y. Bi, X.-L. Du, Y.-M. Liu, Y. Cao, H.-Y. He and K.-N. Fan, *J. Am. Chem. Soc.*, 2012, **134**, 8926−8933; (*g*) A. Boddien, C. Federsel, P. Sponholz, D. Mellmann, R. Jackstell, H. Junge, G. Laurenczy and M. Beller, *Energy Environ. Sci.*, 2012, **5**, 8907−8911; (*h*) K. Koh, J.-E. Seo, J. H. Lee, A. Goswami, C. W. Yoon and T. Asefa, *J. Mater. Chem. A*, 2014, **2**, 20444−20449; (*i*) Y. Chen, Q.-L. Zhu, N. Tsumori and Q. Xu, *J. Am. Chem. Soc.*, 2015, **137**, 106−109.

5 (*a*) Y. Huang, X. Zhou, M. Yin, C. Liu and W. Xing, *Chem. Mater.*, 2010, **22**, 5122−5128; (*b*) S. Jones, J. Qu, K. Tedsree, X.-Q. Gong and S. C. E. Tsang, *Angew. Chem., Int. Ed.*, 2012, **51**, 11275−11278; (*c*) K. Mori, M. Dojo and H. Yamashita, *ACS Catal.*, 2013, **3**, 1114-1119; (*d*) Z.-L. Wang, J.-M. Yan, Y. Ping, H.-L. Wang, W.-T. Zheng and Q. Jiang, *Angew. Chem., Int. Ed.*, 2013, **52**, 4406−4409; (*e*) Y.-Y. Cai, X.-H. Li, Y.-N. Zhang, X. Wei, K.-X. Wang and J.-S. Chen, *Angew. Chem., Int. Ed.*, 2013, **52**, 11822−11825.

6 (*a*) Q.-L. Zhu, N. Tsumori and Q. Xu, *Chem. Sci.,* 2014, **5**, 195−199; (*b*) K. Jiang, K. Xu, S. Zou and W.-B. Cai, *J. Am. Chem. Soc.*, 2014, **136**, 4861−4864; (*c*) S.-J. Li, Y. Ping, J.-M. Yan, H.-L. Wang, M. Wu and Q. Jiang, *J. Mater. Chem. A*, 2015, **3**, 14535−14538; (*d*) Y. Chen, Q.-L. Zhu, N. Tsumori and Q. Xu, *J. Am. Chem. Soc.*, 2015, **137**, 106−109.

7 (*a*) X. Zhou, Y. Huang, W. Xing, C. Liu, J. Liao and T. Lu, *Chem. Commun.*, 2008, **30**, 3540−3542; (*b*) Y. Ping, J.-M. Yan, Z.-L. Wang, H.-L. Wang and Q. Jiang, *J. Mater. Chem. A*, 2013, **1**, 12188−12191; (*c*) M. Hattori, D. Shimamoto, H. Ago and M. Tsuji, *J. Mater. Chem. A*, 2015, **3**, 10666−10670.

8 (*a*) K. Przybylski and W. W. J. Smeltzer, *Electrochem. Soc.*, 1981, **128**, 897−902; (*b*) B. E. Hayden, *Acc. Chem. Res.*, 2013, **46**, 1858−1866; (*c*) H. Mistry, R. Reske, Z. Zeng, Z.-J. Zhao, J. Greeley, P. Strasser and B. R. Cuenya, *J. Am. Chem. Soc.*, 2014, **136**, 16473−16476.

9 (*a*) W. Zhu, R. Michalsky, O. Metin, H. Lv, S. Guo, C. J. Wright, X. Sun, A. A. Peterson and S. Sun, *J. Am. Chem. Soc.*, 2013, **135**, 16833−16836; (*b*) Q. Zhang, I. Lee, J. B. Joo, F. Zaera and Y. Yin, *Acc. Chem. Res.*, 2013, **46**, 1816−1824; (*c*) J. Liu, L. Jiang, B. Zhang, J. Jin, D. S. Su, S. Wang and G. Sun, *ACS Catal.*, 2014, **4**, 2998−3001; (*d*) Z. Zhao, J. Arentz, L. A. Pretzer, P. Limpornpipat, J. M. Clomburg, R. Gonzalez, N. M. Schweitzer, T. Wu, J. T. Miller and M. S. Wong, *Chem. Sci.*, 2014, **5**, 3715–3728; (*e*) S. Zhang, P. Kang and T. J. Meyer, *J. Am. Chem. Soc.*, 2014, **136**, 1734−1737; (*f*) R. Reske, H. Mistry, F. Behafarid, B. R. Cuenya and P. Strasser, *J. Am. Chem. Soc.*, 2014, **136**, 6978−6986.

10 (*a*) Y. Ding, F. Fan, Z. Tian and Z. L. Wang, *J. Am. Chem. Soc.*, 2010, **132**, 12480−12486; (*b*) D. Wang and Y. Li, *Adv. Mater.*, 2011, **23**, 1044−1060; (*c*) C. J. DeSantis, A. C. Sue, M. W. Bower and S. E. Skrabalak, *ACS Nano*, 2012, **6**, 2617−2628; (*d*) J. Gu, Y.-W. Zhang and F. Tao, *Chem. Soc. Rev.*, 2012, **41**, 8050−8065.

11 (*a*) H. Zhang, M. Jin, Y. Xiong, B. Lim and Y. Xia, *Acc. Chem. Res.*, 2013, **46**, 1783−1794; (*b*) N. S. Porter, H. Wu, Z. Quan and Y. Fang, *Acc. Chem. Res.*, 2013, **46**, 1867−1877.

12 (*a*) S. Sarina, H. Zhu, E. Jaatinen, Q. Xiao, H. Liu, J. Jia, C. Chen and J. Zhao, *J. Am. Chem. Soc.*, 2013, **135**, 5793−5801; (*b*) Q. Xiao, S. Sarina, A. Bo, J. Jia, H. Liu, D. P. Arnold, Y. Huang, H. Wu and H. Zhu, *ACS Catal.*, 2014, **4**, 1725−1734.

13 (*a*) B. Lim, H. Kobayashi, T. Yu, J. Wang, M. J. Kim, Z.-Y. Li, M. Rycenga and Y. Xia, *J. Am. Chem. Soc.*, 2010, **132**, 2506−2507; (*b*) J. W. Hong, D. Kim, Y. W. Lee, M. Kim, S. W. Kang and S. W. Han, *Angew. Chem., Int. Ed.*, 2011, **50**, 8876−8880; (*c*) J. S. Jirkovský, I. Panas, E. Ahlberg, M. Halasa, S. Romani and D. J. Schiffrin, *J. Am. Chem. Soc.*, 2011, **133**, 19432−19441.

14 (*a*) X. Gu and D. Xue, *Cryst. Growth Des.*, 2007, **7**, 1726−1732; (*b*) B. Wang, A. P. Côté, H. Furukawa, M. O'Keeffe and O. M. Yaghi, *Nature*, 2008, **453**, 207−211; (*c*) A. Phan, C. J. Doonan, F. J. Uribe-Romo, C. B. Knobler, M. O'Keeffe and O. M. Yaghi, *Acc. Chem. Res.*, 2010, **43**, 58−67.

Through decreasing the size of AuPd nanoparticles, the catalytic activity enhancement in the hydrogen generation from formic acid was achieved.